Journal of Colloid and Interface Science 350 (2010) 381–386

Contents lists available at ScienceDirect

Journal of Colloid and Interface Science

www.elsevier.com/locate/jcis

Colloidal crystal growth monitored by Bragg diffraction interference fringes

Justin J. Bohn, Alexander Tikhonov, Sanford A. Asher *

Department of Chemistry, University of Pittsburgh, Pittsburgh, PA 15260, USA

ARTICLE INFO

Article history:
Received 9 November 2009
Accepted 26 April 2010
Available online 12 June 2010

Keywords:
CCA
Bragg diffraction
Interference fringes
Ordering
Growth kinetics

ABSTRACT

We monitored the crystal growth kinetics of crystallization of a shear melted crystalline colloidal array (CCA). The fcc CCA heterogeneously nucleates at the flow cell wall surface. We examined the evolution of the (1 1 1) Bragg diffraction peak, and, for the first time, quantitatively monitored growth by measuring the temporal evolution of the Bragg diffraction interference fringes. Modeling of the evolution of the fringe patterns exposes the time dependence of the increasing crystal thickness. The initial diffusion-driven linear growth is followed by ripening-driven growth. Between 80 and 90 μM NaCl concentrations the fcc crystals first linearly grow at rates between 1.9 and 4.2 μm/s until they contact homogeneously nucleated crystals in the bulk. At lower salt concentrations interference fringes are not visible because the strong electrostatic interactions between particles result in high activation barriers, preventing defect annealing and leading to a lower crystal quality. The fcc crystals melt to a liquid phase at >90 μM NaCl concentrations. Increasing NaCl concentrations slow the fcc CCA growth rate consistent with the expectation of the classical Wilson–Frenkel growth theory. The final thickness of wall-nucleated CCA, that is determined by the competition between growth of heterogeneously and homogenously nucleated CCA, increases with higher NaCl concentrations.

1. Introduction

Charged, monodisperse colloidal particles suspended in relatively pure water can form randomly dispersed suspensions, crystalline colloidal arrays (CCA), or glassy structures [1–9]. Surface-charged monodisperse colloidal particle suspensions will crystallize into non-close-packed CCA with fcc or bcc structures over wide ranges of particle concentrations, surface charge densities, and salt concentrations [5,6]. The samples can be polycrystalline or they can form large single crystal domains [10–15]. The degree of CCA ordering depends on the colloidal particle size and charge, as well as the particle size and charge monodispersity, the average spacing between particles, and the solution ionic strength, the temperature, and the medium dielectric constant, all of which impact the electrostatic interactions between particles [16–20].

Very low particle charge and/or very high charge screening can result in particle repulsive interactions so small that the thermal kinetic energy of the particles exceeds their primary interparticle repulsive energy barriers. This allows the attractive van der Waals forces to dominate, which results in irreversible particle flocculation [21,22].

Increasing particle charge will electrostatically stabilize colloidal particle dispersions, preventing particle flocculation. For modest electrostatic stabilization the colloidal particles will not show long-range order and, thus, adopt a liquid-like phase with short range ordering [1,2,13,23,24]. At larger electrostatic interactions the particles can self-assemble into well-ordered CCA [1,13,14,25]. The equilibrium particle ordering in this case is generally in an fcc or bcc structure.

Further increases in particle electrostatic interactions can create systems where the interparticle repulsive interactions are too large for the particles to crystallize into highly ordered crystalline states [4]. This is because the electrostatic interactions are too large to allow the particle motion and density fluctuations which enable crystal annealing. The system in this case forms a vitreous glass or an amorphous solid [4,7,9,26–28].

The kinetics of ordering of these glassy and amorphous solid systems can be very slow to nonexistent [4,7,26,27]. However, these systems can be induced to order by applying mechanical perturbations such as shear forces parallel to the container walls that induce particle layer assembly parallel to the walls; the shear forces overcome the activation barriers for particle motion [9,13,14,29–34].

Previous studies of colloidal crystal growth in strongly electrostatically repelling colloidal suspensions show two regimes: linear growth followed by growth by ripening. In the linear crystal growth regime the growth kinetics are controlled by particle diffusion from the melt to the growing colloidal crystal surface. The growth rates of homogeneously nucleated crystals have been measured over a large range of colloidal particle volume fractions as well as increasing salt concentrations at constant colloidal particle volume fractions [13,30–32,35].

* Corresponding author. Fax: +1 412 624 0588.
E-mail address: asher@pitt.edu (S.A. Asher).

0021-9797/$ - see front matter © 2010 Elsevier Inc. All rights reserved.
doi:10.1016/j.jcis.2010.04.072

The growth rates of bcc CCA heterogeneously nucleated at the container cell wall have been measured and found to vary between 0.1 and 10 μm/s for colloidal suspensions of 102 nm diameter particles and 450 charges [36,37]. Increasing the volume fraction of these colloidal particles from 0.0013 to 0.0024 increases the growth rate 1000-fold from 0.01 to 10 μm/s. Increasing the NaCl concentration from 0 to 1.2 μM while holding the colloidal particle volume fraction fixed decreases the colloidal crystal growth rate from 10 to 0.01 μm/s.

From these studies it appears that both homogeneously and heterogeneously nucleated colloidal crystal growth rates follow the Wilson–Frenkel growth law [13,30,35,36,38,39]. There are fewer studies of the growth rates of more strongly electrostatically interacting particles that commonly form fcc CCA.

An understanding of the crystal growth mechanisms of CCA is important for optimizing this growth to form large single domain crystals for use as photonic crystals [11,40–44]. Thin films of these crystals can be used to reject narrow bandwidths of light from the UV to near-IR spectral regions [11,10].

Numerous methods have been used to study the degree of ordering of CCA. Methods utilizing confocal and visual microscopy are able to image colloidal particles in the first few layers of a colloidal crystal [36,45–48].

The CCA Bragg diffraction intensities and bandwidths can provide information on the crystal ordering [48–53]. In the thick crystal limit a decreasing crystal ordering results in a decrease in the Bragg peak intensity and an increase in the angular width. For example, Colvin and co-workers showed that the Bragg-diffracted intensities decrease for close-packed CCA fabricated with increasing colloidal particle size polydispersities [48]. Norris et al. demonstrated for solid close-packed CCA that the interference fringe modulation depths decrease with increasing disorder [54].

In the work here, we examine the growth kinetics of CCA formed from highly charged colloidal particles in suspensions containing different NaCl concentrations. We observe for the first time Bragg diffraction fringes from non-close-packed liquid CCA samples. We use these interference fringes to monitor the growth of the CCA out from the wall where they heterogeneously nucleate.

2. Materials and methods

Our CCA are composed of 200 ± 3 nm diameter polystyrene colloidal particles (2.52×10^{13} particles/cm^3) which each possess 33 000 surface sulfonate groups. We added NaCl to the particle dispersions to partially screen the electrostatic interactions in order to achieve ordering kinetics in the seconds time frame, which is easily studied.

We previously characterized the structure of our CCA without adding NaCl and found them to be fcc [55]. Since the (1 1 1) plane diffraction wavelength did not change with NaCl addition no transition to a bcc structure occurred, indicating that the samples studied here are all in an fcc structure; if an fcc to bcc phase transition occurred due to the NaCl-induced decrease in the electrostatic repulsions between particles the Bragg peak wavelength would have blue-shifted ~25 nm.

We monitored the ordering and growth of CCA from the wall by measuring the relative intensities of the Bragg fcc (1 1 1) diffraction peaks and the interference fringes in the wings of these Bragg diffraction peaks. The fringe spacings are known to depend on the crystal thickness [54,56]. Thus, measurements of the fringe spacings directly indicate the thickness of the growing CCA crystals. As far as we know this is the first report to observe these fringes in liquid CCA samples and the first to utilize their time-dependent spacings to monitor CCA growth kinetics.

Fig. 1 shows the reflection spectrum of an fcc CCA sample of 200 ± 3 nm diameter polystyrene colloidal particles containing 30 μM NaCl illuminated with a collimated white light beam normal to the flow cell container wall, where the light was collected in a backscattering geometry.

We mechanically perturbed this sample by inducing shear flow and then tapped on the container to mechanically disturb the CCA to speed up its crystallization. The peak centered at $\lambda_B = 861$ nm derives from first-order Bragg diffraction from the fcc CCA (1 1 1) planes.

On both sides of the first-order Bragg diffraction reflection peak we observe intensity oscillations which damp off at wavelengths away from the Bragg maximum [49,55,57–59]. These fringes result from the partial constructive interference for light which is backscattered from the (1 1 1) planes within the crystal [57].

The highest particle density fcc (1 1 1) planes orient parallel to the sample cell wall, such that normally incident light travels along the normal to the (1 1 1) planes [2]. The (1 1 1) plane diffraction occurs at $\lambda_B = 2d_{111}n_{avg}\sin\theta$, where λ_B is the wavelength of light in vacuum, n_{avg} is the CCA average refractive index, d_{111} is the (1 1 1) plane spacing, and θ is the glancing angle, that for normal incidence is $\pi/2$ giving $\lambda_B = 2d_{111}n_{avg}$. We calculate a volume-averaged CCA refractive index, $n_{avg} = \varphi_{H_2O}n_{H_2O} + \varphi_{Pst}n_{Pst} = 1.357$, where φ_{H_2O} is the volume fraction and n_{H_2O} is the refractive index of water. φ_{Pst} is the volume fraction and n_{Pst} is the refractive index of polystyrene. We calculate a lattice plane spacing of $d_{111} = 321$ nm.

This fringe pattern can be used to determine the thickness of the CCA fcc crystal. We search for the crystal thickness which gives the best match between the calculated and the observed fringe patterns. We model the CCA diffraction as if it results from a 1-D stack of bilayer dielectric slabs which have periodicities and an overall average refractive index that is identical to those of the CCA [59]. We determined the thicknesses and refractive indices of the dielectric slab bilayers by requiring them to show the same reflectance as that of a single CCA fcc (1 1 1) layer calculated in the kinematic single scattering approximation [59]. Our modeling of Fig. 1 data indicates a total of 90 (1 1 1) layers which yields a 29 ± 0.5 μm CCA thickness.

We examined the time dependence of ordering of a CCA sample within a rectangular 700 μm flow cell. We used a syringe to inject

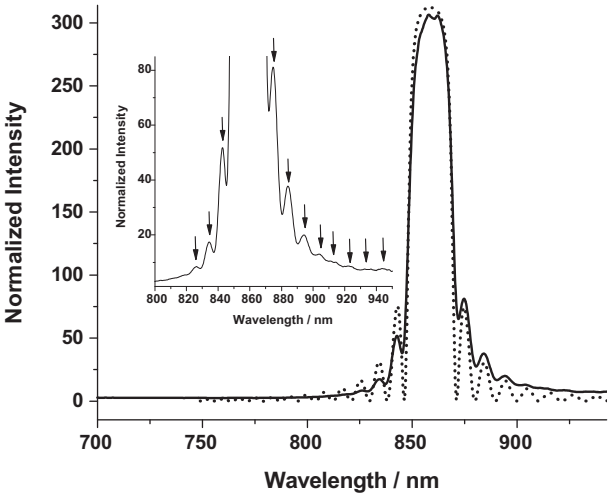

Fig. 1. Normal incidence reflection spectrum from a CCA within a 700 μm thick flow cell. The CCA has a particle number density 23 μm^{-3} and consists of 200 ± 3 nm polystyrene particles in water containing 35 μM NaCl, where each particle contains ~33 000 surface sulfonates. The first-order Bragg diffraction peak at normal incidence from the (1 1 1) planes occurs at 869 nm. The inset shows an expanded region around the first-order Bragg diffraction peak. The dashed line shows the best fit modeling of the fringe pattern which indicates a 29 μm effective crystal thickness.

the CCA into the flow cell and then waited until the CCA ordered to its maximum extent, as monitored by the plateauing of the increasing intensity of the (1 1 1) first-order Bragg diffraction peak. We then perturbed the CCA ordering by injecting more sample such that the sample volume in the flow cell shifted 1 cm down the flow cell, giving a shear rate of $\sim$14 s^{-1} for this 700 μm thick flow cell. We then monitored the diffraction evolution after this perturbation.

For our CCA samples we only observe spontaneously formed fringes in samples with NaCl concentrations between 75 and 90 μM. Samples at higher salt concentrations do not form well-ordered CCA because the electrostatic interactions are too weak for long-range crystalline order. Lower salt concentration samples will show fringes only if they are forced to order by repetitive shear and/or by mechanical tapping on the container wall to force ordering as in Fig. 1.

3. Results

Fig. 2 shows the time evolution of the diffraction and fringe peaks collected at normal incidence for fcc CCA samples with NaCl concentrations of 75, 80, 85, and 90 μM. The time-resolved diffraction measurements are shown as overlapping diffraction spectra acquired every 0.2 s over a 1-min period. We scaled the contrast of the resulting intensity profiles to visually maximize the number of interference peaks observed.

Fig. 2 shows that the number of visible fringes increases with increasing NaCl concentrations up until 85 μM. Fringes do not spontaneously form under these shear flow conditions for NaCl concentrations below 75 μM. These colloidal particle suspensions with NaCl concentrations above 90 μM do not show formation of the diffraction peak over a period of 24 h after injection. A decreasing fringe spacing with an increasing fringe modulation depth indicates a growing, increasingly ordered crystal [56].

Fig. 3a shows the first-order Bragg diffraction peak intensities as a function of time for CCA containing 75, 80, 85, and 90 μM NaCl concentrations. The data show an initial rapid increase in peak intensity for each CCA sample, with very similar initial rates for 75 and 80 μM NaCl, but with decreasing initial rates for the 85 and 90 μM NaCl concentrations. The largest Bragg diffraction peak intensities are achieved for the 85 and 90 μM NaCl concentration CCA. After $\sim$20 s, the 85 and 90 μM NaCl CCA show identical Bragg diffraction peak intensities.

Utilizing the bilayer slab modeling of the fringe pattern as discussed above as a function of time after shear perturbation we calculated the time dependence of the growing crystal thickness (Fig 3b). The 75 μM NaCl CCA sample is not included because fringes were not observed.

In Fig. 3b, 80 μM NaCl CCA thickness shows a rapid initial growth which stops abruptly after 6 s, where the CCA achieves a final thickness of 22 ± 0.4 μm. The 85 μM NaCl CCA sample growth rate is slightly slower than that of the 80 μM NaCl CCA and saturates by $\sim$25 s while achieving a thickness of 43 ± 0.5 μm. The 90 μM NaCl CCA has the slowest growth rate, where the increasing thickness does not saturate within the measured 50 s time frame. At 50 s after shear the 90 μM NaCl CCA thickness increases to 54 ± 0.6 μm.

The reflection intensity of the main Bragg peak in Fig. 1a reaches a plateau after 5–6 s for all our samples. However, from Fig. 3b, we see that the wall crystal thickness for the 85 and 90 μM samples continues to increase after 6 s. The saturation of the main Bragg peak results from reaching the so-called thick crystal limit, the point at which crystal thickness is increased to the point where it diffracts essentially all incident light. Any further increase in thickness cannot affect the Bragg peak intensity. Our slab modeling of diffraction intensity shows that a perfectly ordered 16 μm thick wall crystal should diffract 90% of the incident light. This 16 μm thickness is reached after $\sim$5 s (Fig. 3b).

A simpler method for calculating the crystal thickness based on a kinematic approximation gives essentially the same crystal thicknesses. In this model the intensity of the back-diffracted light is proportional to the structure factor:

$$S(\lambda) = \left[\sum_{m}^{M-1} \exp\left[-im\left(d_{111}\cdot\frac{4\pi}{\lambda}\right)\right]\right]$$

where M is the number of (1 1 1) planes having a well-defined inter-plane spacing. We calculate the thickness of ordered CCA along the (1 1 1) normal by calculating the number of (1 1 1) planes involved in the diffraction, which is

$$M = 2\pi\left\{d_{111}n_{avg}\left(\frac{4\pi}{\lambda_1}-\frac{4\pi}{\lambda_2}\right)\right\}^{-1}$$

where λ_1 and λ_2 are adjacent fringe peak wavelengths. The thickness of the ordered fcc CCA is $T = (M-1)d_{111}$. In Fig. 3c we calculated the crystal thickness by using fringe pairs furthest away from the Bragg diffraction peak. We get crystal thicknesses very similar to Fig. 3b. The fringe pairs spacing decreases for interference fringes closer to Bragg diffraction peak because of multiple scattering effects [57,58]. Therefore, fringe pairs closer to the Bragg diffraction peak give slightly larger calculated crystal thicknesses.

4. Discussion

4.1. CCA growth

Application of shear to the CCA sample disorders the system which causes the Bragg diffraction peak to disappear. The Bragg diffraction peak reappears immediately after cessation of shear, indicating prompt crystal nucleation at the wall. The evolving interference fringe patterns in Fig. 2 indicate that after cessation of shear a CCA crystal of uniform thickness (over the measured 0.5 cm diameter spot size) grows out from the wall [37]. Homogeneous nucleation appears to also occur within the bulk of the colloidal suspension giving rise to growing randomly orientated CCA domains which eventually stop the growth of the wall-nucleated CCA [30,37,60].

In Fig. 3b the CCA thickness time dependence can be separated into three regions. The first region corresponds to a rapid and linear initial growth from the cell wall. These initial growth velocities decrease with increasing NaCl concentrations (4.2, 2.3, and 1.9 μm/s for the 80, 85, and 90 μM NaCl CCA samples).

According to classical Wilson–Frenkel growth theory the growth rate follows $v = v_\infty(1-\exp(-\Delta\mu/k_BT))$, where v_∞ is the limiting velocity and $\Delta\mu$ is the chemical potential difference between the melt and the crystal. Palberg and co-workers calculated the Wilson–Frenkel growth velocity of a growing bcc CCA using the DLVO interaction potential between colloidal particles and found that the growth velocity decreases with increasing salt concentration [36]. Our experimental observation are consistent with the Wilson–Frenkel law dependence [35,61,62]. The linear CCA growth is due to colloidal particle diffusion from the liquid-like phase to the growing colloidal crystal surface where it adds to help grow the crystal [13].

The wall crystal growth was measured by Wette et al. in a relatively dilute system where the equilibrium crystal structure is bcc [63]. They observe a delay in the heterogeneously wall-nucleated crystal growth. This may result from the requirement of a recrystallization of the flow-induced rhcp structure to the final equilibrium bcc structure. Our results for a more concentrated system do not show a delay in the wall crystal growth. This could be because the evolution from the rhcp structure to the fcc structure requires only registering of the hexagonal planes. In addition,

Bragg diffraction from the fcc (1 1 1) planes may not significantly differ from that of the rhcp stack.

The second region spans the time period between when the growth begins to slow and when the growth begins to stop. The slowing growth probably occurs due to contact of the growing CCA from the wall against homogeneously nucleated CCA crystallites within the bulk [37]. Fig. 3b shows that second region time span increases with increasing NaCl concentrations. At 80 μM NaCl the second time region lasts ∼5 s. For 85 μM NaCl the second growth span time interval increases to 25 s. The time span is longest for the 90 μM NaCl CCA where the CCA thickness continues to grow past our entire measurement time period.

The CCA continues to grow out from the wall in region 2 even after contacting the homogeneously nucleated crystallites probably due to a crystal ripening phenomenon whereby larger CCA crystals grow at the expense of smaller CCA crystallites [64,65]. Colloidal particles melt from smaller CCA domains and attach to larger CCA domains [65]. The particles that transfer from small to large crystallites must surmount electrostatic repulsion activation energy barriers which decrease as the NaCl concentration increases.

Thus, ripening is expected to result in the slowest region 2 growth for the 80 μM NaCl CCA. Increasing the NaCl concentration to 85 and 90 μM NaCl decreases the activation barriers which should increase the growth rate compared to that at lower NaCl concentrations. In region 3 the entire sample volume has crystallized, ripening has dramatically slowed because there are no small crystallites left.

Fig. 3d shows a log–log plot of the crystal thickness growth data of Fig. 3b. We find a $t^{1/3}$ power law dependence as shown by the thin lines. The initial region of crystal growth in Fig. 3d shows a slope corresponding to a t^1 power law. The second ripening region for the 80 and 85 μM salt samples show a $t^{1/3}$ power law, which is expected for the Lifshitz–Slyozov coarsening behavior found for systems with conserved order parameters [39,64,65]. There is a transition region between the t^1 and the $t^{1/3}$ growth regions, probably because of the combination of the diffusion-controlled Wilson–Frankel growth mechanism and coarsening crystal growth mechanism [39]. For the 80 μM salt sample we also see another region at the longest times when crystal ripening growth gradually stops and the wall crystal thickness remains constant over the measured time interval. Our data for 85 and 90 μM salt samples unfortunately do not extend long enough to monitor this region where the crystal thickness stops growing.

4.2. CCA ordering quality

The number of interference fringes and their relative intensities depend on the quality of the CCA ordering. Interference fringes require that the CCA crystal has a well-defined number of uniformly spaced well-ordered crystal layers. Decreasing layer ordering and uniformity will decrease the modulation of the interference fringes making them less evident [54]. Therefore, we can utilize the interference fringe pattern to monitor CCA ordering.

Interference fringes do not appear for CCA with NaCl concentrations <75 μM in the absence of mechanical perturbations. The fringes only spontaneously appear for our CCA samples with NaCl concentrations between 80 μM and 90 μM NaCl (Fig. 2b), indicating that at these salt concentrations the CCA are able to nucleate

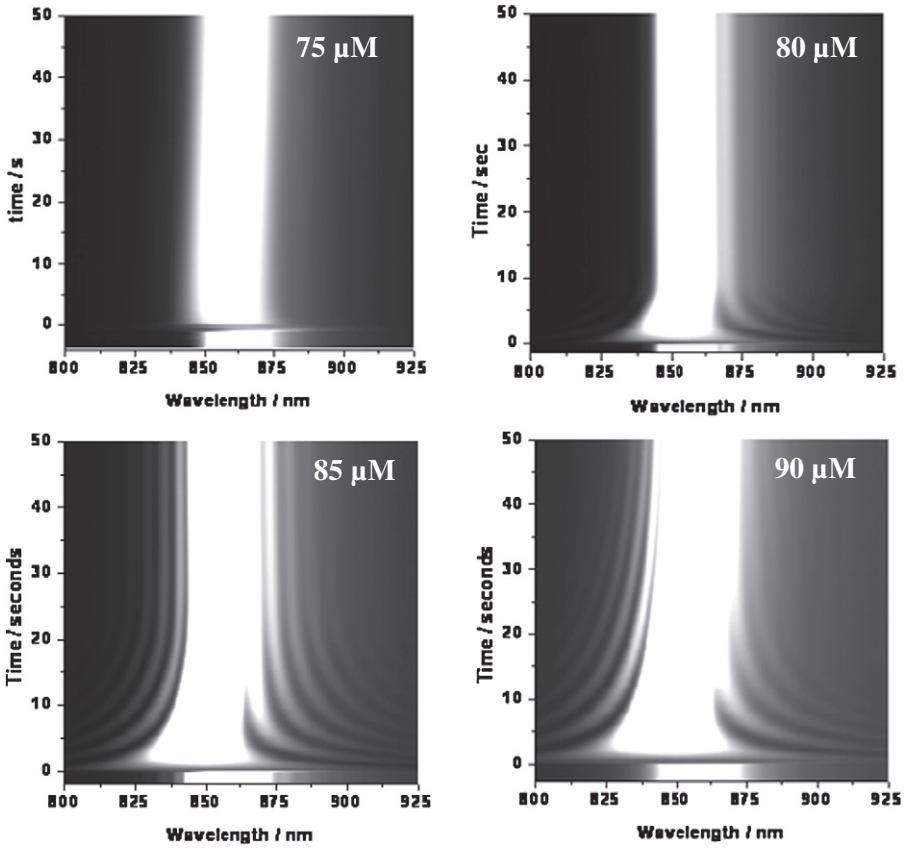

Fig. 2. Diffraction intensity as a function of time for the first-order Bragg diffraction from the fcc (1 1 1) planes observed at normal incidence for four CCA samples containing 75 80, 85, and 90 μM NaCl concentrations. The data show the annealing process of the CCA after shear flow is applied to the CCA. The lighter bands surrounding the first-order Bragg diffraction peak show the fringe pattern evolution as the CCA thickness increases. The intensities were scaled to maximize the fringe visibility.

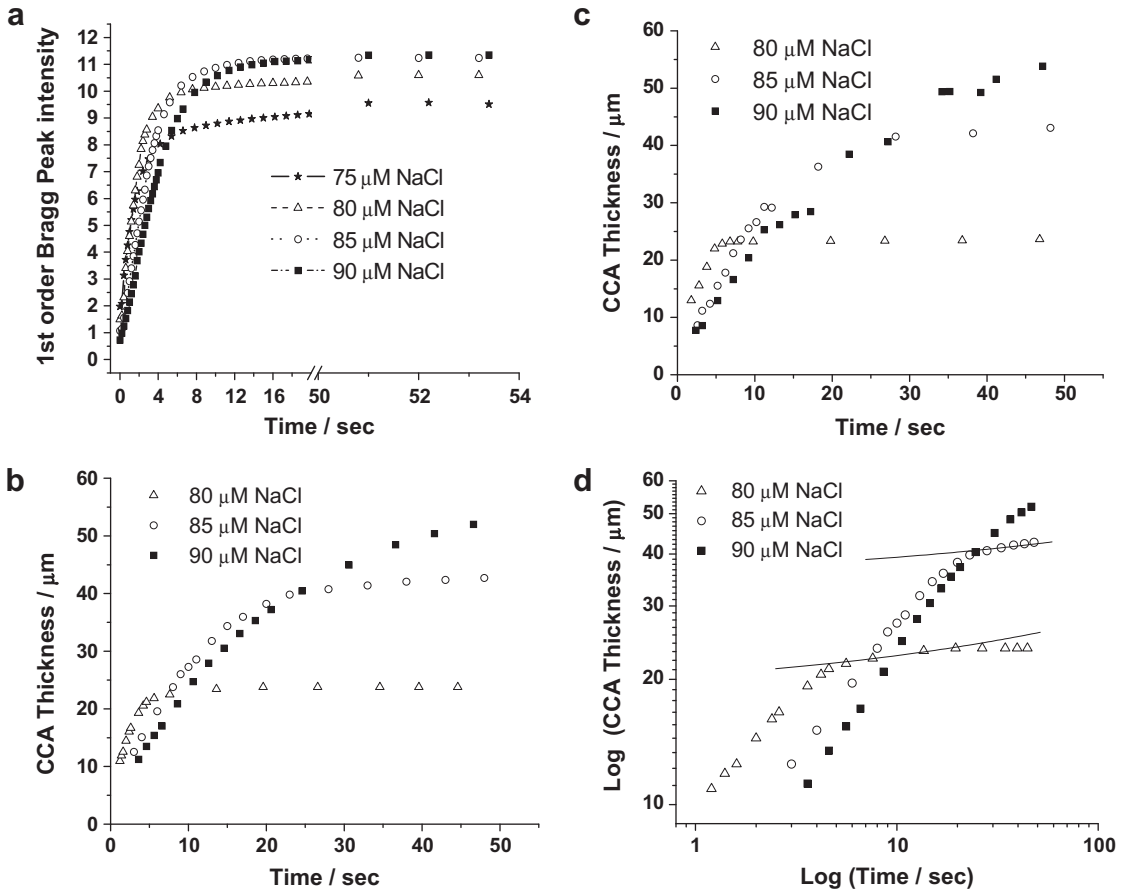

Fig. 3. Wall crystal growth kinetics after cessation of shear flow at time zero. (a) Time dependence of Bragg diffraction peak reflected intensity for CCA containing different NaCl concentrations. (b) Modeled time dependence of calculated crystal thickness for CCA samples containing different NaCl concentrations. See text for details. (c) Time dependence of estimated crystal thickness using simplified kinematic model. See text for details. (d) Log–log plot of (b).

at the wall and anneal into well-ordered crystals. The improved ordering of these CCA is also signaled by increased Bragg diffraction intensities compared to those at the lower NaCl concentration CCA. In the thick crystal limit larger Bragg intensities indicate less diffuse scattering and better crystal ordering [66].

The 85 μM NaCl CCA shows the largest number and most modulated interference fringes indicating that it is best ordered. There are fewer, less visible fringes for the 90 μM NaCl CCA, although the Bragg diffraction intensities and widths are identical. The interference fringes appear to be a more sensitive indicator of crystal order than the Bragg diffraction intensities and bandwidths.

The decreased ordering of the higher concentration 90 μM NaCl CCA presumably results from the fact that we are approaching salt concentrations where the CCA melts. The poorer ordering of the lower salt concentration CCA in the absence of mechanical perturbation obviously results from the slow crystallization kinetics due to high activation barriers for annealing [44,64,67].

Different crystal defects can differentially impact the visibility of the interference fringes. Interference fringes become less visible if there is a variation in spacing between hexagonal layers, or if the (1 1 1) layers are distorted from the shape of an ideal plane. Thus, the fringes will become less visible if the incident light simultaneously samples several domains with a different numbers of layers. Therefore our method based on monitoring interference fringes is limited to the single domain crystals of relatively high quality. Stacking faults and different stacking of layers will have little or no effect on interference fringes.

The lack of well-ordered wall-nucleated crystals for CCA samples containing NaCl concentrations below 80 μM results in a lack of visible fringes. At low salt, defects do not spontaneously anneal because the relatively high electrostatic interactions between colloidal particles freezes kinetic annealing processes. For intermediate salt concentrations the crystals can be forced to anneal by application of mechanical perturbations such as shearing and tapping. By repeated shearing and mechanical tapping we were able to obtain interference fringes for the 35 μM NaCl sample as shown in Fig. 1.

Typical light scattering experiments to determine the size of a growing crystal measure the width of the Bragg peak for a colloidal crystal having low dielectric contrast between the colloidal particles and the solvent. For these low contrast systems incident light is only weakly attenuated by the crystal. To achieve low dielectric contrast, special index matching techniques were often employed. In contrast, when the dielectric contrast becomes so large that the attenuation length is comparable with the size of a crystal, multiple scattering effects become important and crystal size cannot be determined from the width of the Bragg main peak. Paradoxically the same high value of dielectric contrast, that precludes obtaining the crystal size from the width of the main Bragg peak, helps us to determine crystal thickness from spacing between interference fringes, since the higher the dielectric contrast, the higher the interference fringe intensities.

4.3. Bragg diffraction blue shift

On shearing the 75, 80, 85, and 90 μM samples the Bragg diffraction peaks disappear. After shearing the Bragg peak of the growing wall-nucleated CCA crystal is initially blue-shifted relative

to that before the shear by 2, 3.5, 7, and 9 nm, respectively (Fig. 2). The Bragg peak then red-shifts until it reaches its previous equilibrium value. This Bragg diffraction blueshift probably results from a shear flow-induced colloidal particle concentration increase at the wall which equilibrates over time after cessation of shear. The concentration increase can result from the flow-induced elastically strained shear layers, which was previously observed by Palberg and Biehl [68]. The magnitude of the blue shift decreases as NaCl concentrations decrease because larger electrostatic repulsive interactions increase the resistance to particle concentration increases.

These shear-induced particle concentration increases result in elastic energy storage within the CCA. After the shear forces dissipate this stored elastic energy drives the system back toward a homogeneous particle concentration, which causes the lattice constant and the resulting Bragg peak to relax back to its equilibrium value. All but the 90 μL NaCl sample fully relaxes within 1 min. The 90 μL NaCl sample takes longer, probably, in part, because of its smaller Young's modulus which resulted in a larger concentration increase as indicated by the larger diffraction blue shift. In addition, it is possible that crystal melting could be involved in storing elastic energy which would give rise to a long time constant relaxation.

The relaxation back to equilibrium is similar for the 80, 85, and 90 μM samples with a fast relaxation (∼5 s) followed by a much slower relaxation (∼1 min). The 75 μM NaCl sample relaxation differs from the other samples because it continues to blue shift for ∼5 s after cessation of shear. This suggests an additional stage of elastic response where a new source of elastically stored energy after cessation of shear continues to increase the particle concentration near the wall. We will continue to examine this process which occurs in CCA which have larger interparticle electrostatic interactions.

5. Conclusions

We monitored the growth of fcc CCA heterogeneously nucleated at the cell wall after shear melting by monitoring the Bragg diffraction intensities, and for the first time, the Bragg interference fringe patterns. Modeling of the evolution of the fringe patterns exposes the time dependence of the increasing crystal thickness. Between 80 and 90 μM NaCl concentrations the fcc crystals grow from the wall at rates between 1.9 and 4.2 μm/s until they contact homogeneously nucleated crystals in the bulk. At lower salt concentrations crystal nucleation is slow because the strong electrostatic interactions between particles result in high activation barriers preventing annealing. The fcc crystals melt to a liquid phase at >90 μM NaCl concentrations. Increasing NaCl concentrations slows the fcc CCA growth rate in accordance with the expectations of the classical Wilson–Frenkel growth theory.

Acknowledgments

This work was funded by NIH Grant RO1EB004132 and NSF Grant CHE-8048265.

References

[1] P.A. Hiltner, I.M. Krieger, J. Phys. Chem. 73 (1969) 2386.
[2] R. Kesavamoorthy, S. Tandon, S. Xu, S. Jagannathan, S.A. Asher, J. Colloid Interf. Sci. 153 (1992) 188.
[3] R.J. Carlson, S.A. Asher, Appl. Spectrosc. 38 (1984) 297.
[4] E.B. Sirota, H.D. Ou-Yang, S.K. Sinha, P.M. Chaikin, J.D. Axe, Y. Fujii, Phys. Rev. Lett. 62 (1989) 1524.
[5] Y. Monovoukas, A.P. Gast, J. Colloid Interf. Sci. 128 (1989) 533.
[6] P.N. Pusey, W. Van Megen, Nature 320 (1986) 340.
[7] W. van Megen, S.M. Underwood, Nature 362 (1993) 616.
[8] L. Cipelletti, L. Ramos, J. Phys. Condens. Matter 17 (2005) R253.
[9] F. Sciortino, P. Tartaglia, Adv. Phys. 54 (2005) 471.
[10] P.L. Flaugh, S.E. O'Donnell, S.A. Asher, Appl. Spectrosc. 38 (1984) 847.
[11] S.A. Asher, P.L. Flaugh, G. Washinger, Spectroscopy (Springfield, OR) 1 (1986) 26.
[12] T. Okubo, Polym. J. (Tokyo, Jpn.) 40 (2008) 882.
[13] T. Palberg, J. Phys. Condens. Matter 11 (1999) R323.
[14] N.A. Clark, A.J. Hurd, B.J. Ackerson, Nature 281 (1979) 57.
[15] A. Van Blaaderen, P. Wiltzius, Adv. Mater. (Weinheim, Ger.) 9 (1997) 833.
[16] A. Yethiraj, A. van Blaaderen, Nature 421 (2003) 513.
[17] P. Pieranski, L. Strzelecki, B. Pansu, Phys. Rev. Lett. 50 (1983) 900.
[18] W. Van Megen, I. Snook, Adv. Colloid Interface Sci. 21 (1984) 119.
[19] M.O. Robbins, K. Kremer, G.S. Grest, J. Chem. Phys. 88 (1988) 3286.
[20] A. Yethiraj, Soft Matter 3 (2007) 1099.
[21] W.B. Russel, D.A. Saville, W.R. Schowalter, Colloidal Dispersions, Cambridge University Press, New York, 1989.
[22] P.C. Hiemenz, Principles of Colloid and Surface Chemistry, second ed., Dekker, New York, 1986.
[23] T. Okubo, J. Phys. Chem. 93 (1989) 4352.
[24] J.C. Zahorchak, R. Kesavamoorthy, R.D. Coalson, S.A. Asher, J. Chem. Phys. 96 (1992) 6873.
[25] R. Kesavamoorthy, B.V.R. Tata, A.K. Arora, A.K. Sood, Phys. Lett. A 138 (1989) 208.
[26] P.N. Pusey, W. Van Megen, P. Bartlett, B.J. Ackerson, J.G. Rarity, S.M. Underwood, Phys. Rev. Lett. 63 (1989) 2753.
[27] H.J. Schope, T. Palberg, J. Non-Cryst. Solids 307–310 (2002) 613.
[28] H.J. Schope, T. Palberg, Progr. Colloid. Polym. Sci. 118 (2001) 82.
[29] W. Khunsin, G. Kocher, S.G. Romanov, C.M. Sotomayor Torres, Adv. Funct. Mater. 18 (2008) 2471.
[30] D.J.W. Aastuen, N.A. Clark, L.K. Cotter, B.J. Ackerson, Phys. Rev. Lett. 57 (1986) 1733.
[31] B.J. Ackerson, N.A. Clark, Phys. Rev. A 30 (1984) 906.
[32] J. Vermant, M.J. Solomon, J. Phys. Condens. Matter 17 (2005) R187.
[33] A. Van Blaaderen, MRS Bull. 29 (2004) 85.
[34] W.D. Dozier, P.M. Chaikin, J. Phys. 43 (1982) 843.
[35] T. Okubo, S. Okada, J. Colloid Interf. Sci. 192 (1997) 490.
[36] M. Wuerth, J. Schwarz, F. Culis, P. Leiderer, T. Palberg, Phys. Rev. E 52 (1995) 6415.
[37] A. Stipp, R. Biehl, T. Preis, J. Liu, A.B. Fontecha, H.J. Schoepe, T. Palberg, J. Phys. Condens. Matter 16 (2004) S3885.
[38] T. Okubo, A. Tsuchida, T. Kato, Colloid Polym. Sci. 277 (1999) 191.
[39] Y. He, B.J. Ackerson, W. van Megen, S.M. Underwood, K. Schaetzel, Phys. Rev. E 54 (1996) 5286.
[40] S. John, Phys. Rev. Lett. 58 (1987) 2486.
[41] E. Yablonovitch, J. Phys. Colloq. C5 (1987) C5.
[42] A. Blanco, E. Chomski, S. Grabtchak, M. Ibisate, S. John, S.W. Leonardo, C. Lopez, F. Meseguer, H. Miguez, J.P. Mondia, G.A. Ozin, O. Toader, H.M. Van Driel, Nature 405 (2000) 437.
[43] S. Noda, K. Tomoda, N. Yamamoto, A. Chutinan, Science 289 (2000) 604.
[44] K. Ito, H. Nakamura, H. Yoshida, N. Ise, J. Am. Chem. Soc. 110 (1988) 6955.
[45] B.V.R. Tata, B. Raj, Bull. Mater. Sci. 21 (1998) 263.
[46] U. Gasser, E.R. Weeks, A. Schofield, P.N. Pusey, D.A. Weitz, Science 292 (2001) 258.
[47] V. Prasad, D. Semwogerere, E.R. Weeks, J. Phys. Condens. Matter 19 (2007) 113102.
[48] R. Rengarajan, D. Mittleman, C. Rich, V. Colvin, Phys. Rev. E 71 (2005) 016615.
[49] E. Palacios-Lidon, B.H. Juarez, E. Castillo-Martinez, C. Lopez, J. Appl. Phys. 97 (2005) 063502.
[50] Y.A. Vlasov, V.N. Astratov, A.V. Baryshev, A.A. Kaplyanskii, O.Z. Karimov, M.F. Limonov, Phys. Rev. E 61 (2000) 5784.
[51] V.N. Astratov, A.M. Adawi, S. Fricker, M.S. Skolnick, D.M. Whittaker, P.N. Pusey, Phys. Rev. B 66 (2002) 165215.
[52] J.F. Galisteo Lopez, W.L. Vos, Phys. Rev. E 66 (2002) 036616.
[53] A.V. Baryshev, V.A. Kosobukin, K.B. Samusev, D.E. Usvyat, M.F. Limonov, Phys. Rev. B 73 (2006) 205118.
[54] Y.A. Vlasov, M. Deutsch, D.J. Norris, Appl. Phys. Lett. 76 (2000) 1627.
[55] A. Tikhonov, J. Bohn, S. Asher, Phys. Rev. B 80 (2009) 235125.
[56] P. Jiang, J.F. Bertone, K.S. Hwang, V.L. Colvin, Chem. Mater. 11 (1999) 2132.
[57] A. Yariv, Y. Pochi, Optical Waves in Crystals: Propagation and Control of Laser Radiation, Wiley-Interscience, New York, 1984.
[58] H. Miguez, V. Kitaev, G.A. Ozin, Appl. Phys. Lett. 84 (2004) 1239.
[59] A. Tikhonov, R.D. Coalson, S.A. Asher, Phys. Rev. B 77 (2008) 235404.
[60] R. Blaak, S. Auer, D. Frenkel, H. Loewen, J. Phys. Condens. Matter 16 (2004) S3873.
[61] H.A. Wilson, Philos. Mag. 50 (1900) 238.
[62] J. Frenkel, Phys. Z. Sowjetunion 1 (1932) 498.
[63] P. Wette, A. Engelbrecht, R. Salh, I. Klassen, K. Menke, D.M. Herlach, S.V. Roth, H.J. Schope, J. Phys. Condens. Matter 21 (2009).
[64] S. Iacopini, T. Palberg, H.J. Schoepe, Phys. Rev. E 79 (2009) 010601.
[65] S. Iacopini, T. Palberg, H.J. Schoepe, J. Chem. Phys. 130 (2009) 084502.
[66] W.H. Zachariasen, Theory of X-Ray Diffraction in Crystals, Dover, New York, 1967.
[67] C. Haro-Perez, L.F. Rojas-Ochoa, R. Castaneda-Priego, M. Quesada-Perez, J. Callejas-Fernandez, R. Hidalgo-Alvarez, V. Trappe, Phys. Rev. Lett. 102 (2009) 018301.
[68] T. Palberg, R. Biehl, Faraday Discuss. 123 (2003) 133.